Material Selection & Design for Lattice-based Biodegradable Metal Implants for Bone Regeneration in Load-Bearing Bone Defects

Shantanab Dinda[1], Dishary Banerjee[2], Derek Shaffer[3], Ibrahim T. Ozbolat[2], and Timothy W. Simpson[1]

[1]Department of Industrial & Manufacturing Engineering
[2]Department of Engineering Science & Mechanics
[3]Department of Material Science & Engineering
The Pennsylvania State University, University Park, PA, 16802

Abstract

Human bone is a dynamic tissue and has a natural ability to repair small fractures quickly; however, critical fractures below the waist require external mechanical aids to help bear loading while healing. These techniques are effective but tend to cause a lack of mobility and decrease quality of life. New materials focused on the biodegradability of implants have opened new avenues in implant design and fabrication, reducing previous concerns such as tunability of degradation rates in such materials. Furthermore, three-dimensional (3D) printed biodegradable metallic implants show promise as an alternative for expediting recovery and increasing mobility, especially with the growth of lattice-based design and better osseointegration techniques. This study discusses the development and testing of a functional AM implant that integrates load-bearing, biodegradability, biocompatibility, and osseointegration, with an eye toward clinical translation. Based on the desired material properties, an iron-manganese mixture is used, along with dopants to aid biocompatibility and improve degradation rates. Lattice-based design has been implemented to reduce material usage without affecting mechanical properties, and the implants have been printed using binder jetting. After fabrication, experiment analysis to evaluate mechanical properties, degradation rates and byproducts, in-vitro performance, and microstructure has been performed for validation, to prepare the implant for in-vivo testing, giving us a functional lattice-based biodegradable metal implant.

Introduction

Bones are built for fast repair in the event of bone loss or fracture. This can occur in partial or segmental fractures due to excessive or unbalanced loading on the bone, or when the bone has to be voluntarily removed due to scenarios such as cancer or necrosis [1]. To accomplish bone repair, the fracture site induces granular tissue growth from each end of the fracture, and these then extend into the fracture area and come together to form a connection known as *bridging* [2]. However, bridging has its limitations when it comes to large sections of bone loss or complex fractures. This limitation in bridging due to the gap being too big is defined as a critical defect [3], and external help is needed for the correct alignment and repair of the bone in question [4].

External repair and alignment techniques for simpler fracture cases such as braces and casts are in use for sites where loading is not necessary for movement (such as arm fractures) [5], but there are additional issues when it comes to fractures below the waist, as the techniques need to deal with the repair, alignment, and load from body weight and movement, as the mechanical requirements are still present despite the fracture [2,4]. External help is needed to mitigate the loading requirements. Current Methods like casts, rods, and plates do ensure that the foot is arrested in the correct alignment and load is transferred, but there are several disadvantages to these methods. These fixtures are permanent in the case of rods and plates and may cause toxicity issues [6,7]. In some cases, while arresting the foot, such measures tend to overcompensate for the load. This is known as stress shielding and can cause bone loss [8]. In some cases, especially with pediatric or geriatric patients, conditions such as rapid growth or osteoporosis may hamper bone growth and repair, as well as cause further bone damage when internal devices like plates and rods have been used that need to be attached to the bone surface [9].

Additionally, dealignment during fracture healing is also a possibility with any external method, and should also be considered before it's too late in the healing process, this can cause incorrect healing and permanent misalignment [10]. These issues can be mitigated with the use of implants designed and implanted in the body to address one or more of the points. Bone repair with implants requires 3 aspects: 1) The size and geometry that meets the physical requirements of the fracture site, and in the case of load-bearing location, also contribute to mitigating the loading requirements [11,12], 2) Seeding the implant with stem cells, that would grow and aid with bridging [13], 3) Providing signaling molecules to convert stem cells to bone, also known as osteoblasts [13,14].

Several different techniques exist for constructing implants. Some of this is done by using the patient's bone through allogeneic procedures and composite bone grafting [15]. But they have limitations in how much bone can be extracted, strength, flexibility, and cost. Polymer and ceramic implants have become common now, and offer a lot of versatility in terms of design and manufacturability due to the use of additive manufacturing (AM) [16], however, such implants are unable to meet the mechanical requirements needed for a load-bearing implant. Metallic Implants are best for load bearing, and with the help of AM, are now showing better porosity (for promoting cellular growth deeper in the implant) and surface interaction with the adjacent bone, allowing for better attachment and reducing chances of dealignment [10]. However, for metallic implants, there are limitations in materials considering the functional requirements, and as most such implants are permanent, thus any sort of metal leaching from them can be toxic to the body in the quantities that are needed for such an application [8]. Based on these requirements and limitations in different repair techniques and types of implants, it is possible to isolate the features that are desired from an implant that would be suitable for such an application and location. Considering issues like mechanical strength, permanency, and toxicity, we can consider some specific features to be desirable in an implant: load bearing, biodegradability, biocompatibility, and osseointegration. A lot of research has gone into implant development, but a major shortcoming of studies only focuses on only one or some of these features at a time. Some research focuses purely on the biological performance and how stem cells would grow on an implant and differentiate into bone cells [14], while others focus more on the design, fabrication, and mechanical performance aspects [17]. It would be ideal for the metallic implant to degrade gradually as the fracture heals and the loading requirements can be sustained by the native bone over time, and the implant integrates with the surrounding bone so that the stem cells can grow and integrate with the native bone. Such features can be accentuated with the design and fitment of the implant [18]. Furthermore, the growth of AM allows lattice-based design and better osseointegration techniques, as it allows greater design flexibility via the use of design for AM concepts and the possibility of light-weighting [19].

There is considerable research in this area but focused more on the degradation and biological performance aspects rather than design, even for AM cases [17]. The focus of this paper is to combine such desired features and incorporate them into a single implant. However, combining biocompatibility, degradability and AM leads to limited choices in materials considering the functional requirements [20]. To achieve this successfully, this paper has a systematic approach to making such a functional implant: choosing materials and dopants to enhance desired properties [20], accessing their biocompatibility and printing, and incorporating lattice-based design to enhance several properties. After fabrication, the implant is evaluated in several areas such as mechanical testing, degradation, *in-vitro* work, and microstructure analysis for performance validation, some of which are discussed in this paper, while others will be evaluated in the future study. It is imperative for better performance and good clinical translation, as the implant must be functional in the end [21]. The study will be geared towards *in-vivo* analysis for lower (rats) and higher (goat/sheep) animals, with the final steps focused on evaluating the clinical performance of such an implant, giving us a functional lattice-based biodegradable implant.

The remainder of the paper is organized as follows. First, the materials used for the fabrication of such an implant are discussed, along with the experimental methods used for each of the stages in the paper. This section discusses both the work established in the literature and its verification, and the novelties introduced by the paper in the form of materials, design, and fabrication. Next, the results and inferences from the various experiments and design work are discussed, along with an overview of the iterative design and fabrication process. Finally, the final section outlines the plans for this work and how it would be continued in a subsequent study.

Materials & Methods

The study this paper covers has been split into five stages. The first stage establishes the scope of the study, based on understanding the mechanical constraints and requirements, the material properties for the major components of the implant, and selecting the printing process. With the boundary conditions and limitations set, the study moves to the second stage: a preliminary biological study stage to evaluate the biological and degradation performance of the main constituents of the implant. The third stage is aimed at assessing the printability of the powders and establishing the sintering parameters. These three stages work as a cyclic platform, with changes being made iteratively if needed. After the verifications were completed, additional elements for improving certain characteristics in the implant are researched and introduced in varying quantities. The implant is then printed with these variations (without design considerations), sintered, and its biological performance is assessed for each case. Once the ideal composition of dopants is established, the study moves to the design and simulation of lattice-based implants on nTopology [22] instead of the solid model used so far, with their fabrication and sintering. Preliminary testing has been done on such implants in terms of microstructure analysis (SEM and EDS), along with degradation analysis using ICP-AES. The approach used in this study focuses on establishing feasibility in Stages 1-3, then moves to combine various desired features systematically.

Stage I

Mechanical Constraints

As mentioned previously, the transition from native bone to a metallic implant must be able to sustain the load in the section of bone it is replacing. Load-bearing bones have three major regions (Figure 1): the hard compact bone which sustains most of the load and is the stiffest component, the softer trabecular bone inside the compact bone which is spongy, and the bone-marrow which doesn't contribute to load-bearing, rather generate the different cellular components of blood [23]. For this paper, only the loading on the compact bone is considered for mechanical properties, as it sustains most of the load in a standard scenario.

Stress due to gravitational pull and simple loading is usually compressive, but there are exceptions where loading from varying directions can occur (dynamic loading). For establishing loading constraints, three elements are considered in literature based on human testing: the young's modulus, strain rate, and bone density [24]. Based on this data, a range of load on the bone is determined that mimics the variation in compressive and dynamic loads, giving rise to multiple loading cases and scenarios. Based on the analysis, a pressure between 4 and 10 MPa is seen to generate the normal load during simulation and design, depending on the strain rate.

A simpler yet holistic approach has been considered to determine the load, where a normal compressive load on the top surface of the implant covering the worst-case scenario for loading (10 MPa) is applied, and the bottom surface is constrained. The implementation of this is discussed further in the design section. A critical takeaway here would be that due to the density and superior compressive strength of metals, a smaller volume of metals is needed, relative to the volume of the bone it is replacing. For more advanced studies considering dynamic loading, an implant that can compensate for such loading will have to be designed, but without the issues of overcompensation seen in current non-AM implants.

Printing Process Selection

Considering that the implant incorporates lattice-based design and light-weighting, AM is necessary to fabricate it. This also allows one to vary the implant for dimensional and abstract geometrical variations. Customization is not being considered at this stage. It's preferable to select a printing process that does not induce phase changes or cause extensive changes in parameters, or excessive sintering: leading to excessive interparticle bonding, making degradation slower. Considering these requirements, Binder Jetting was selected. Binder Jetting is ideal as it offers low sintering, which will improve degradation rates [25]. Though the process has a low resolution and no environmental control, these issues don't affect the desired properties and functionality of such an implant.
In addition to this, virgin powder is used in mixture form for printing, instead of alloying and then ball milling or atomizing to get alloyed powder as it gives a wide range of powder diameter, and may affect the feature size and mechanical performance when printing lattices [26].

Material Selection

Material selection is dependent on the ability to print with powder from these metals, their biocompatibility, and the possibility of such metals degrading without harming the body. Choices based on printability are abundant, especially with the possibility of printing using several different processes. However, the need for biocompatibility and degradability heavily constrain the choices. Three types of components constitute such an implant. The primary component fulfills the desirable features such as printability, degradability, mechanical strength, and historical use for medical purposes, especially *in-vivo* or clinical experimentation. Based on these requirements and literature, only iron and magnesium are viable candidates for the primary component. Biologically, magnesium is the better choice, and both perform well mechanically [27]. However, Magnesium can degrade rapidly and fail, cause gas evolution, and is very difficult to print with as it may combust [28]. Iron, on the other hand, helps with vascular functions and dissipates through blood, and gives better control of the degradation rate [21].

The secondary component's major function is to make the primary component more biocompatible, and usually, they work in pairs. Based on the literature, Iron is paired with Manganese, while Magnesium is paired with Aluminum. Manganese was selected by default here as iron is the primary component. Initially in the study, polymer composites like polycaprolactone (PCL) were also considered as an option, but they were, unfortunately, difficult to structure and degraded too fast, relative to a primary metallic component [27]. Thus, from this pick, iron provides mechanical strength and degradation, while manganese provides biocompatibility. The most commonly used components in literature are 70% iron and 30% manganese [21]. For this study, it was decided that the based composition will be the same, but will be tested both for biocompatibility and printability (discussed in the following sections). Once the primary and secondary components are evaluated to be performing satisfactorily in these aspects, additional elements would be added to them as dopants (less than 3%).

***Stage II:* Biocompatibility & Initial Degradation Analysis**

The objective of this step is to evaluate how degradable and biocompatible such elements are, independent of any printing. Samples were fabricated using casting for this portion of the study. Printability, design, and mechanical properties were not considered at this stage. Since manganese tends to vaporize and precipitate at temperatures above 1200°C [29], casting was performed in a sealed environment. No visual traces of vaporization and precipitation after casting.

After casting, the samples were obtained from fragments, with each seeded with 30000 rat mesenchymal stem cells (MSC) to perform a biocompatibility cell study using Live/Dead assay and evaluate cell proliferation and toxicity over 7 days, with Day 4 and Day 7 as evaluation time points. Fluorescent and SEM imaging was also performed at each time point.

For day 1, successful seeding of the samples is observed (Figure 1 (a), (b) & (c)). By day 4, nuclei are visible as well (blue) in fluorescent imaging (Figure 1(d)), and the green spread indicates proliferation. This is better indicated by SEM (Figure 1(e)), which shows strand-like growth that is extracellular matrix (ECM), indicating that the cells are proliferating, and trying to get together to form a tissue. By day 7, it appears that

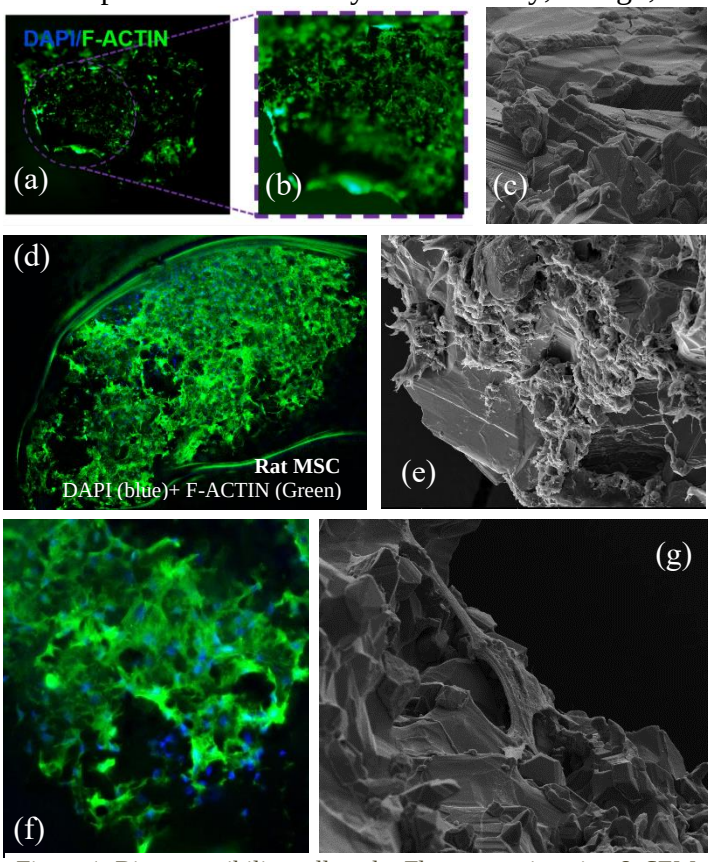

Figure 1: Biocompatibility cell study: Fluorescent imaging & SEM

the ECM has grown even further, indicating good proliferation. Proliferation was also accessed quantitatively, with a cytotoxicity study done for each time point and cell viability appears to grow by 20% for each period, as seen in Figure 2. Thus, based on this experimental study, it is acceptable to consider the iron-manganese combination at this composition to be biocompatible.

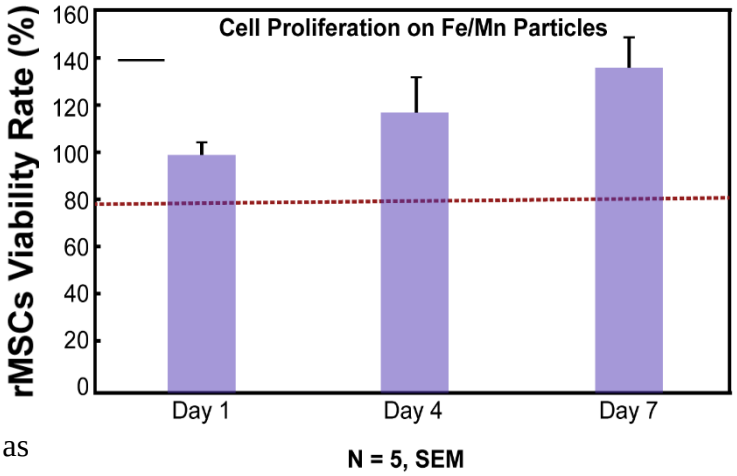

Figure 2: Cell viability rate for Day 1, 4 & 7

For degradation, separate fragment samples were immersed in MSC growth media and Phosphate-buffer Saline (PBS) for 28 days. No visible degradation was seen in these cases, as well as from the cell study and there was minimal change in weight, which was similar to what is expected from casted samples. This shows that the bonding between particles for a casted part is too strong for an implant where degradation is required, and thus it also reiterates the need for lightly sintered parts such as those fabricated using binder jetting.

Stage III: **Printability Assessment & Sintering**

For printing, iron and manganese powders were mixed in the 70-30 composition, both 10 µm in diameter. The printing was done on an Ex-One Innovent+ system with a basic pellet design of 1 cm diameter and 25 mm height, as shown in Figure 3(a). This was selected partially based on the ASTM E09 standard [30], and also for *in-vitro* testing in a 96 well well-plate in later cell studies. Though it was observed that the printing process needed to be optimized for good quality prints, this was not done at this stage but delayed to the design stage as quality would matter the most when lattice-based designs are printed. The green parts were then baked for 4 hours at 180°C for drying the binder. But as seen here, this still means that the parts are held weakly together by a binder (Figure 3(b) and (c)). Additional sintering would be needed to make the parts stronger and prevent delamination, which can occur easily as such samples will be used in aqueous solutions.

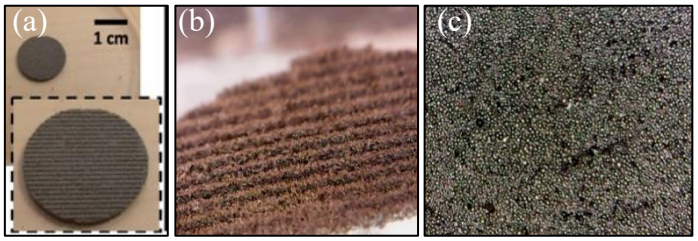

Figure 3: Printed sample with surface texture and quality

Sintering in binder jetting is done using sintering cycles based on the materials and binder used. The cycles have two objectives: to remove the binder residue entirely by burning them out, induce sintering between particles, and improve their density [31]. Additional factors such as the desired properties of the material based on the phase of its components also need to be considered [31]. Based on the phase diagram in Figure 4, compositions between 29% and 47% (the region in red) are preferred as they give a fully austenitic structure or gamma iron. Any lesser would lead to ferrite, or alpha iron formation, which is magnetic (not preferred in an implant [31]) and less

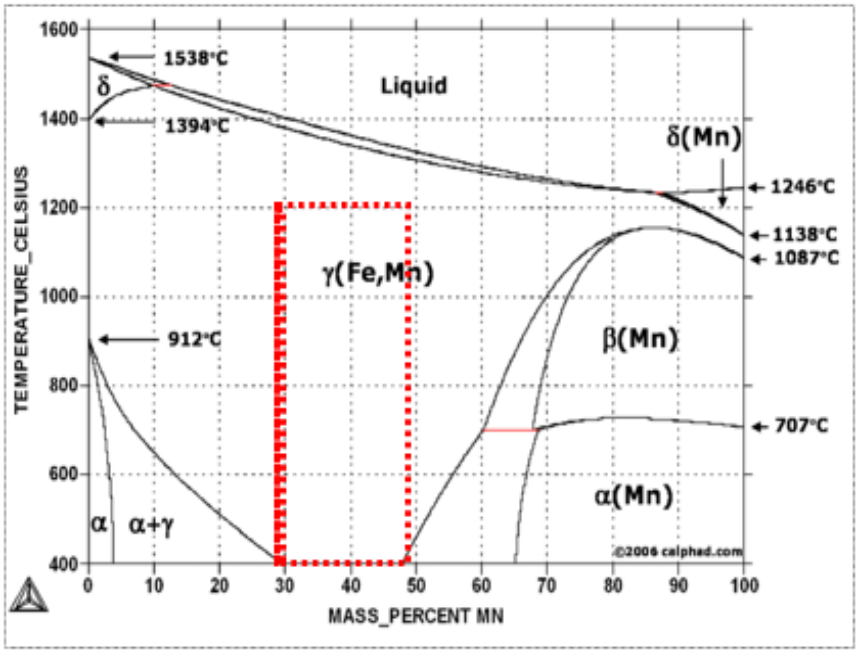

Figure 4: Iron-Manganese phase diagram & sintering zone [29]

dense, possibly making the structure weaker [32]. Sintering above 1200°C was not attempted as the manganese can vaporize. Though it seems sensible to counter this by using a higher concentration of manganese, manganese in high concentrations causes neurological issues [33], thus, exposure to a large quantity may have negative long-term effects on the body, and would also make the implant structurally weaker as the amount of iron goes down as the manganese goes up. Based on this literature and multiple iterations of sintering, the final cycle was developed with 30% manganese as the optimum choice. The final cycle is shown in Figure 5, with a 30 minutes hold at 500°C for debinding, and a 3-hour hold at 1200°C for partial sintering in a reduced environment of 5% Hydrogen and 95% Argon, with hydrogen being used only after the debinding phase. An initial 7-11% shrinkage was seen in the samples, which is expected to be higher in the case of lattice-based implants due to open porosity [34].

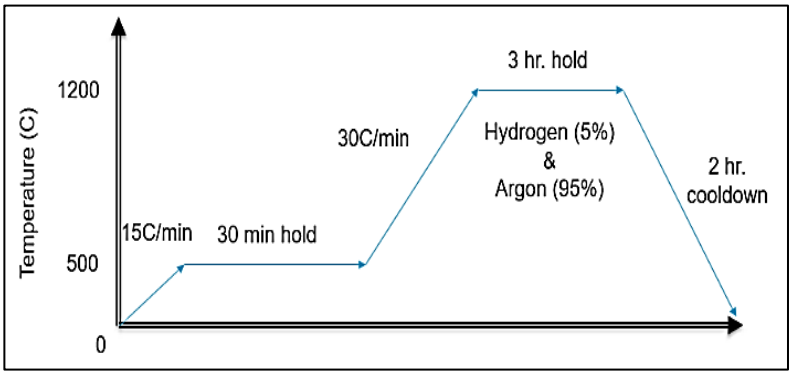

Figure 5: Final sintering cycle

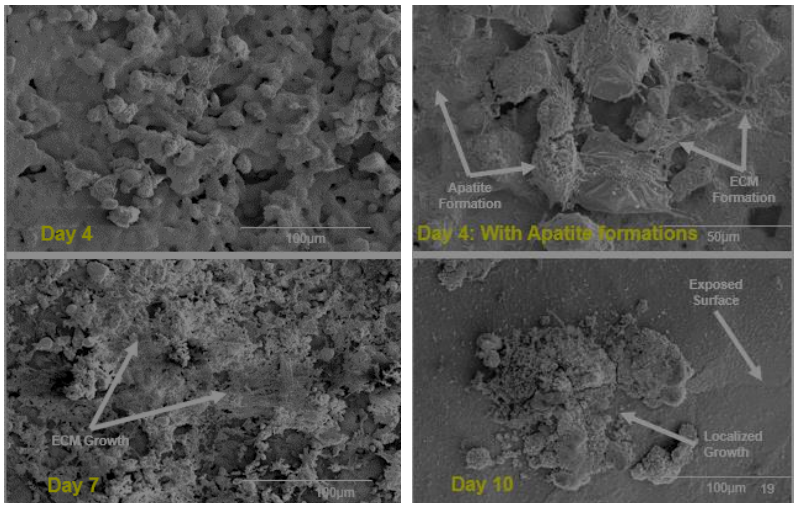

Figure 6: Granular apatite formation and surface loss due to degradation in Iron-Manganese only implant

Stage IV: Dopant Selection & Testing

With the iron-manganese composition set at 70%-30% respectively, dopants were added at this stage while removing the same amount of iron in its place. This was done to improve the degradation rate, cell adhesion, and sterilization. Control in degradation was especially critical due to previous results obtained from the iron-manganese-only samples. Figure 6 shows the initial 10-day study done with just iron-manganese as the constituents, the days 4,7, and 10 as timepoints. Extensive granular apatite formation on every sample with progression in time, possibly due to the presence of phosphate in the growth media which is precipitating as salt particles here. Good proliferation and ECM formation is seen early on, with it growing further on Day 7, with ECM strands visible. However, by Day 10, it is seen that the sample tends to degrade with the surface flaking away, with the surface now visible and cells washed away and now only present in pockets. Considering these features, silicon, silver, and copper have shown promise in enhancing properties in previous studies. The silicon was selected to enhance bone growth and calcification, important considering there is no calcium in the implants [27]. The silver was selected as it reduces the failure of the implant due to bacterial infections and increases in-vivo shelf life, which will be critical during animal trials [35]. The copper was picked as it helps with new blood vessel formation (angiogenesis and vascularization) [27]. Samples either contained Silicon + silver or silicon + copper. Copper and silver weren't added together due to their interactions in sintering [36]. Since these elements can only be used in trace amounts and can be toxic in higher doses, cell studies with human MSCs were conducted with varying amounts of each element for 7 days with timepoints of Day 3 and Day 7, to establish an appropriate concentration at which proliferation is highest. This was done by measuring cellular metabolic activity (MTT) and SEM for quantitative and qualitative analysis respectively. The MTT was done with cells without any implant as the negative control, and the previously used 70-30 composition of iron-manganese as the positive control. Silicon was evaluated first as it is present in all samples, and once the silicon concentration was fixed, silver and copper were each evaluated with the previously fixed percentage of silicon incorporated into the composition. MTT and SEM were performed again to establish the final compositions for each case. Preliminary degradation analysis of the byproducts was also performed at this stage using Atomic Electron Microscopy (ICP-AES).

Concerning non-cellular evaluation, SEM and energy dispersive X-ray spectroscopy (EDS) was used to evaluate the internal composition of the samples after sintering, and to see how the different components evaluate against each other. This method was selected instead of microstructure analysis due to the relatively low density of the implant and partial sintering, preventing compaction and grain growth. The scans were conducted on an Apreo S from Thermo Fisher Scientific with a FEG source and an Ultim Max 100 EDS detector from Oxford Instruments. A beam setting of 15 kV and 1.6 nA was used to obtain full spectrum EDS data for the elements of concern and retain a good signal for the in-column back-scatter detector. A secondary electron detector (ETD detector) was also used to gain better images and detail on porosity in the samples since the secondary electrons are more surface sensitive in comparison to the EDS and back-scatter mapping which are more sensitive to elemental contrast.

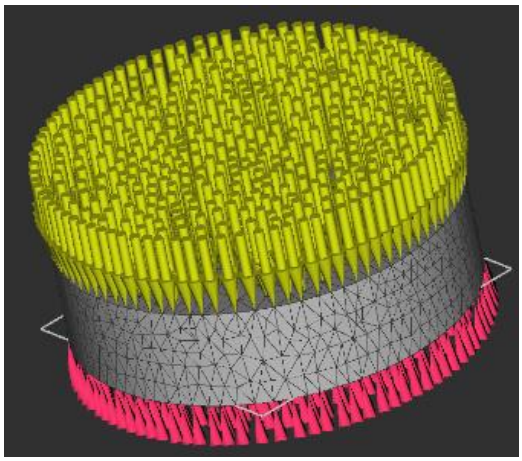

Figure 7: Loading and constraining in base sample

***Stage V:* Design, Simulation & Fabrication**

With several properties evaluated and incorporated at this stage, the study moved to the design stage and incorporated lattice-based design using nTopology, a software specifically adept at handling lattice-based design and simulation. The primary objective of design and simulation is that the implant must sustain the load for the segment of the bone they are replacing. The solid model has used a reference of performance to achieve this considering the loading conditions discussed in Stage I. Based on the calculations done in stage I, the normal force on the top surface of the implant was calculated to be 1.5kN for the lowest strain rate, with the bottom constrained in the direction of the force, as shown in Figure 7. Despite the simplicity of such a scenario, there are some limitations in the material property when simulating in n-topology, primarily as the material used is a mixture, whose inherent properties are difficult to mimic, as well as its density. With this analysis, the lattices present in the lattice library of the software were used with these conditions, and the successful designs moved forward to the printing phase. Printing parameter adjustments were done at this stage to try to print as many of the designs as possible, as well as to observe the possibility of sintering such designs without loss or damage. Only when a design passes the simulation conditions and is possible to print and sinter multiple times is it considered a successful design up to this stage, with subsequent studies focused on testing functionality.

Results & Discussion

When considering the experimentation discussed in the previous section, several key inferences can be made about the composition and the design of these implants.

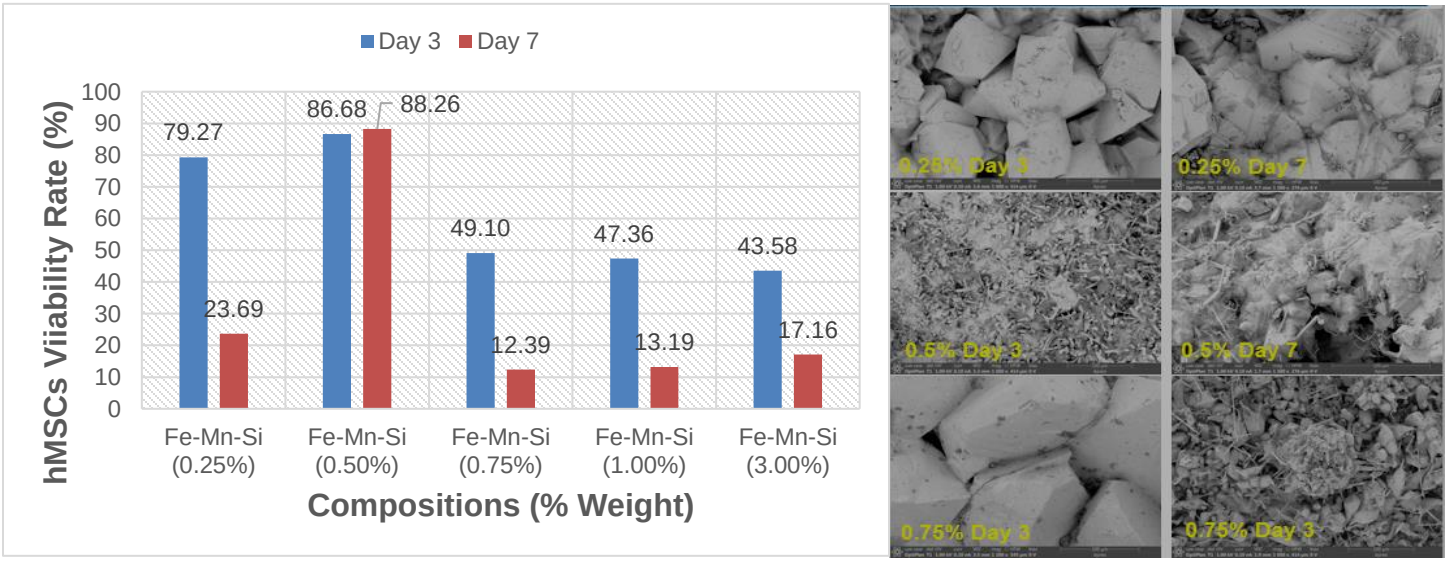

Figure 8: Cell Viability & SEM for Estimating Appropriate Silicon Concentration

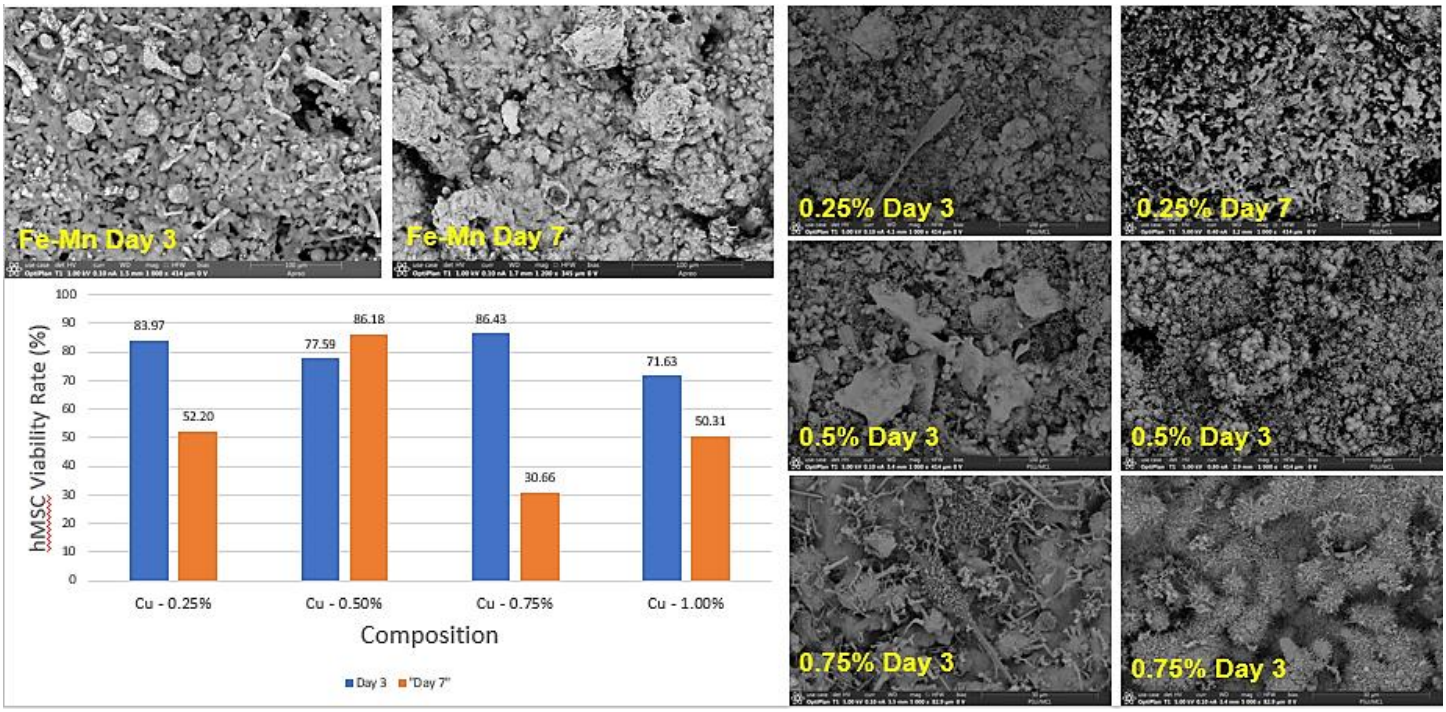

Figure 9: Cell Viability & SEM for estimating appropriate copper concentration

Figure 8 shows the MTT results for the different concentrations used to determine the ideal composition for silicon from various options. Based on this data, it is seen that over 7 days, it's 0.5% silicon by weight which is the least toxic to the cells. One should note that the best results for viability will always be given by undoped samples, but the dopant is present here to enhance other properties, at the expense of marginal loss of cell viability. This was further corroborated based on SEM. SEM was performed for each composition, it is seen that there is a lot more proliferation in 0.5% when compared to the others, while in the case of 0.75% we see extensive apatite formation that looks rather similar, except that hardly any cells or ECM are visible.

With the silicon fixed at 0.5%, the copper composition was evaluated with a similar MTT assay (Figure 9). Similar results were obtained, with 0.5% as the best choice. An important thing to note here is that Day 7 is critical for this analysis, as 7 days is a significant enough period for toxicity to set in, as compared to 3 days, as Day 3 data is pretty similar here for every composition. This was further corroborated based on SEM. Figures 9 (a) & (b) are from the control of just Fe-Mn for Day 3 and Day 7 respectively and are used here for comparison. From this it is seen that 0.5% gives the least apatite formation, thus killing fewer cells by Day 7, as compared to the clusters one can see for 0.25% and 0.75%. Finally, the MTT was also performed for silver cases, and this time the compositions had to be extended to 1.5% to get the ideal case. From Figure 10, it is seen that the relative absorbance is poor for all cases except for 1.5%. Silver is toxic to cells in general, so the results are what one would expect for such a scenario.

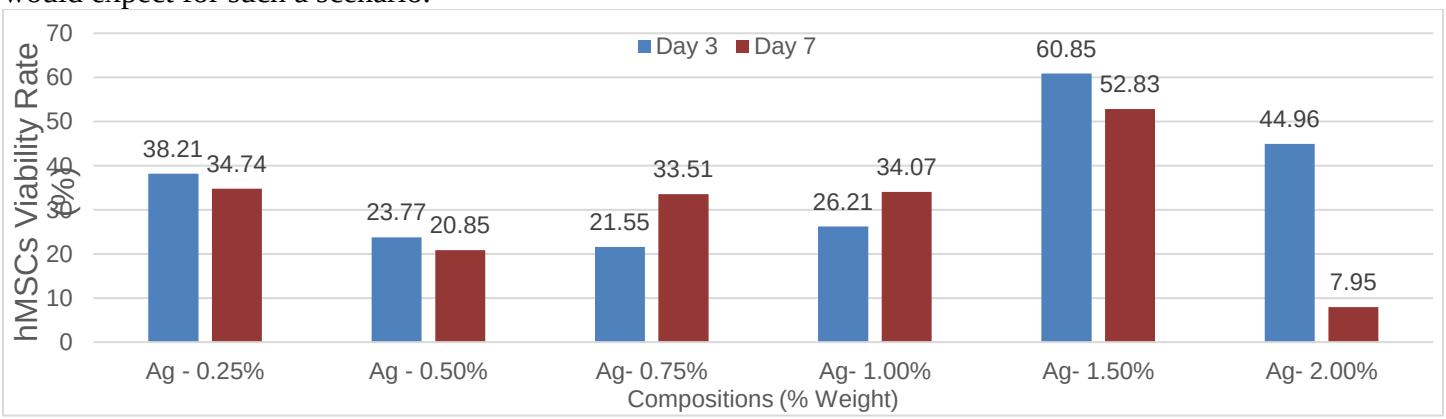

Figure 10: Cell Viability for Estimating Appropriate Copper Concentration

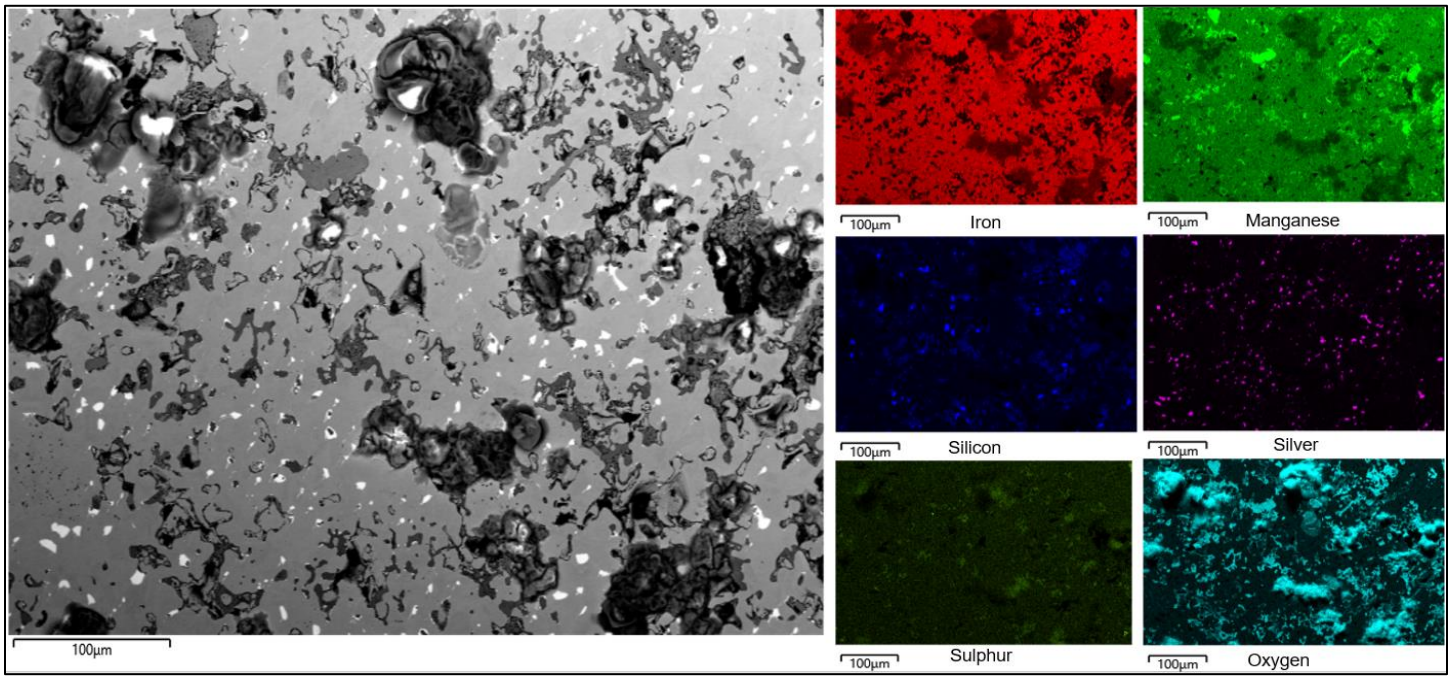

Figure 11: Energy dispersive X-ray spectroscopy (EDS) on Silver-based Implant Samples

EDS was also performed at this stage once the dopant quantities were fixed. Other than the constituent elements, Sulphur and Oxygen were also evaluated due to the presence of oxides and sulfides in metal powders [37]. In the case of silver, it is seen from the SEM image in Figure 11 that the silver doesn't diffuse entirely into the iron matrix. This, however, isn't expected to have any structural impact with such sizes. Furthermore, several oxygen pockets can be seen in this case, along with some manganese and silicon concentrated areas as well. In the case of copper, the dissolution of manganese, copper, and silicon is much better compared to the previous case, as seen in Figure 12. Oxygen is also less prominent in the case of the copper sample, indicating possibly more impurities in silver. Such abnormalities are expected to be present as these are powder mixtures partially sintered together, even if the powder is mixed well initially, and no zones are observed where components are entirely missing.

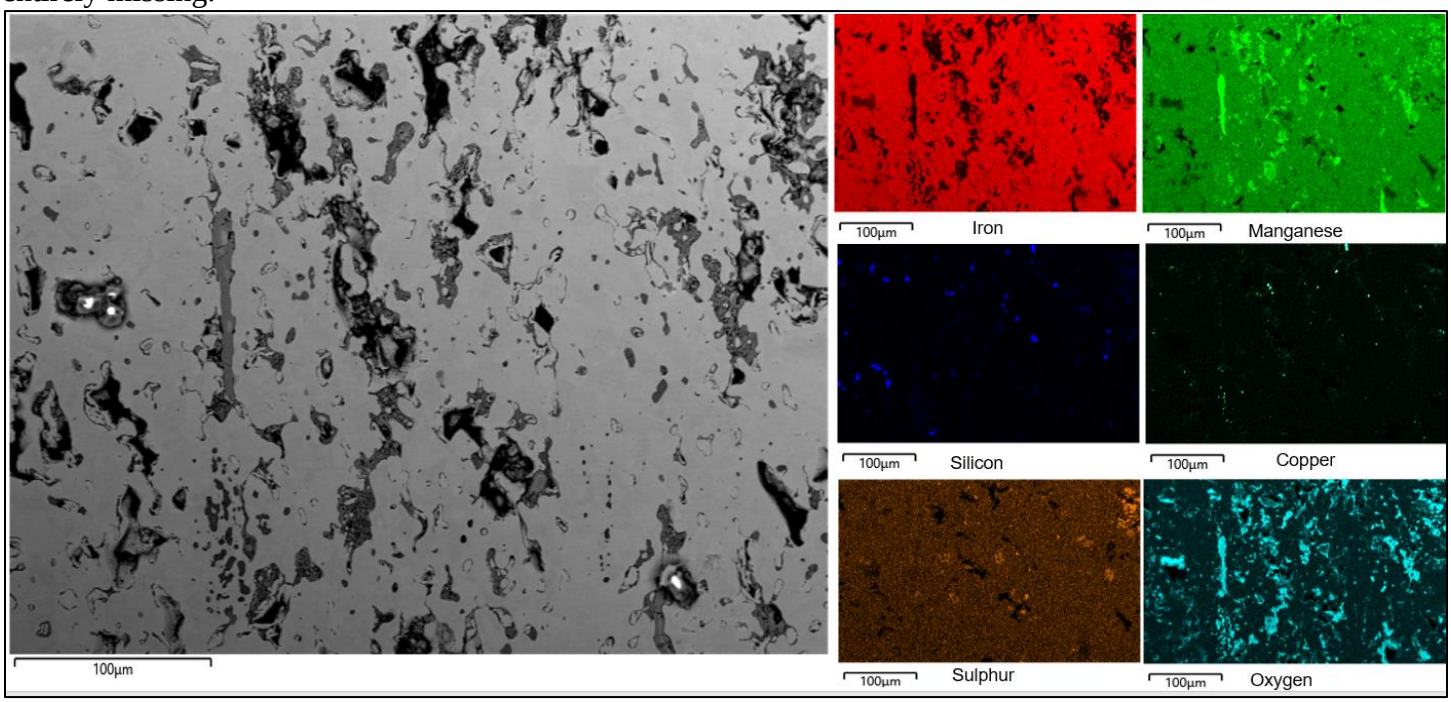

Figure 12: Energy dispersive X-ray spectroscopy (EDS) on Copper-based Implant Samples

Considering the implant is degradable, it's also necessary to experimentally evaluate the degradation effects of dopants. Visual confirmation of degradation for each is seen in Figure 13 and through SEM. For preliminary quantitative analysis, ICP-AES was performed on these to evaluate the particles in the media where the degraded byproducts collect in. The dataset is not large enough for any significant conclusions and will be expanded on in future studies, but as seen in Table 1, the presence of Mn is found to be lower than what is expected, while the others are similar to the initial concentrations. Unfortunately, no silver could be detected, which can be explained by the relatively less diffusion of silver, whereas the others were found to be in similar quantities to what was expected. Further analysis is required as the results can vary depending on the amount and the region of degradation, and the quantification needs to be done with time as a variable.

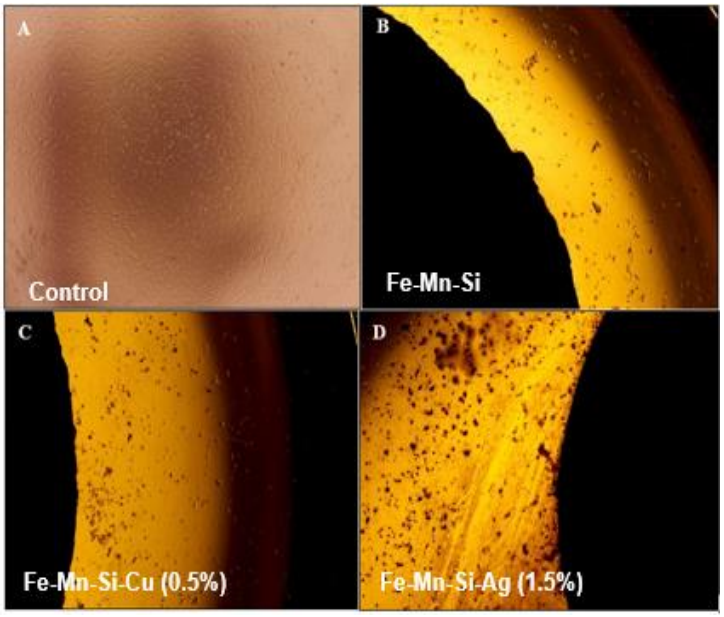

Figure 13: Degradation of Implant in Media and Byproducts

Table 1: ICP-AES Concentrations

Sample	Ag	Cu	Fe	Mn	Si
Silver (1.5%)	<0.01	<0.01	169	30.4	1.08
Copper (0.5%)	<0.01	0.010	158	27.1	1.00

It's imperative to calculate the porosity and density of such samples to understand the limitations of the designs that can be sustained with such material and be printed and sintered successfully. For this purpose, the actual shrinkage and the apparent porosity were calculated using Archimedes, for the basic Iron-manganese samples and the samples with the dopants, but it was seen that all the cases mimic the values of the Silicon-only sample, as despite being just 0.5% by weight, the low density of silicon powder causes enough silicon to be present to appear to make a difference in the outcome. Shrinkage was found to be 38.8% and 36.15% respectively, while the apparent porosity with dopants seems to almost double the value from 22.59% to 44.7%, which can be attributed to open porosity. This can help promote osseointegration and bone growth. These were then considered during simulation, as well as printing parameter alterations.

With this data, the study now moves to the simulation phase, covering the basic case simulation discussed in the previous section. With an initial finite element analysis (FEA), it is seen that the load is concentrated on the top surface instead of dissipating adequately into the implant (Figure 14(a)), with displacement along the top edge, instead of it being spread further down uniformly (Figure 14(b)). Basic buckling analysis was also done, with stress found to be concentrated on the top edge instead of dissipating about the center and causing an expected bulge (Figure 14(c)). These indicated that lattice-based designs would enable the implant to be less stiff and buckle more. This would be especially useful for high strain rates when shock absorption would be necessary.

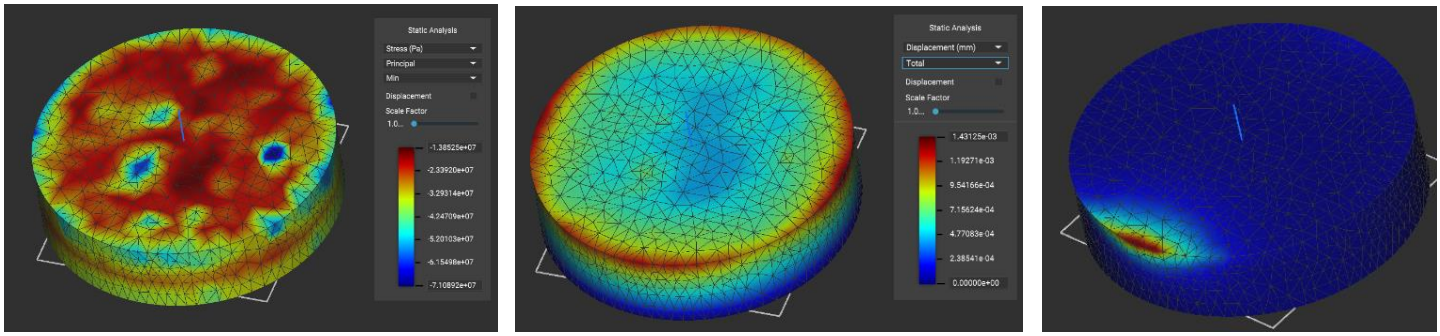

Figure 14: Finite Element Analysis for Basic Cylindrical Implant Structure (No Lattices)

For implementing lattice-based design, 3 aspects are critical: the type of unit cell that will be populated in the part, the location of the nodes, and the thickness of struts and surfaces. Generally, a specific lattice cell is selected, its node altered or specified if needed, and then the thickness of its struts is defined. These choices impact a lot of relevant factors, especially open porosity. Open porosity is different from the sintering density and is purely based on design choices [38]. The impact of node location in bone implant applications is best seen in this example, of the same cell type with a slight difference in displacement. The image in Figure 15 on top has a closed node on the bottom while open ends are on the top. These open ends give it more points for osseointegration, but the closed nodes give fewer points of contact with the print bed. The reverse is seen in the lower case, making printing easier but possibly affecting some aspects of osseointegration. Nodes also play a role in open porosity, as the more nodes, the lesser the pore size. One of the features of osseointegration is the need for more porosity, and thus the placement of nodes is critical for that. This is also seen in the design of AM for hip implants as bone integration is key in joints and weight-bearing areas [8].

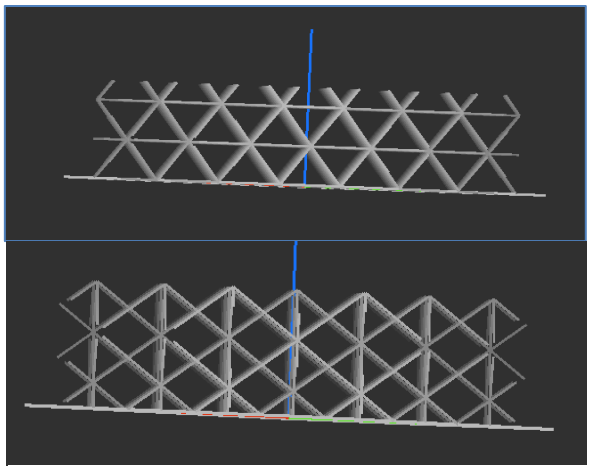

Figure 15: Variation in Node Locations

Based on the literature and the lattice library in nTopology, 18 different lattices were considered for simulation, from which 10 designs were generated based on node locations and dissipation of the load (Table 2). From this, 6 designs showed promise after the simulation was completed using the compressive loading conditions (marked in bold). These designs then entered the printing and sintering phase. Though it was possible to print with each, it was necessary to alter the printing parameters every time, giving a unique set of print parameters for each design. This makes this step unnecessarily complicated, as it would be preferable to have a comprehensive set of parameters that can be used to print most or all current and future designs. With this approach, the print parameters were set and 3 designs (marked in bold and italicized) gave good prints and were also possible to replicate. However, the sintering of such designs without cracking or collapse causes major problems in fabricating lattice-based structures with thin struts. It is seen that most structures with 2mm struts fail during sintering, and in some cases, the 3 printable structures also failed. However, certain alterations in the design, including changes in node points, and non-uniformity in thickness to strengthen certain areas that warp more than the others permitted the parts to be sintered to an acceptable standard. The strengthening was done with the help of the ramping function on nTopology, which allowed variation of thickness along a beam with gradation, as shown in the example in Figure 16. Ramping is useful to control implant degradation, as the thinner sections would degrade first. Thus, the thickened central regions can degrade slower and in a more controlled fashion, reducing the possibility of the implant collapsing prematurely due to uncontrolled degradation.

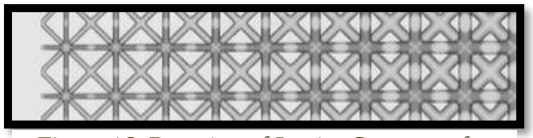

Figure 16: Ramping of Lattice Structures for Beam Strengthening and Controlled Degradation

Table 2: Different lattice Cells that were used for simulation and their printing and sintering outcomes

Type of Design/Lattice	Base Avg. Beam Thickness	Printability
Solid (Control)	NA	Good
Gyroid TPMS Cell (Top)	2mm	Occasional Failure
Gyroid TPMS Cell (Centered)	2mm, 3mm, 5mm	Failure
Gyroid TPMS Cell (Porous)	2mm	Poor finish
Volumetric + Vornoid (Top)	3mm	Unstable structure
Volumetric + Vornoid (Porous)	3mm	Failure during sintering
Volumetric (Asymmetrical + Top)	3mm	Consistency issues
Gyroid TPMS Cell	2mm	Good
Gyroid TPMS Cell (Centered)	2mm, 3mm, 5mm	Good (Except the 2 mm)
Volumetric (Symmetrical + Top)	3mm	Good
Volumetric + Vornoid (Centered)	3mm	Good

Future Work

Additional work is needed to move the implants toward clinical testing. To achieve this, several different types of experiments over a diverse set of fields are required. Aspects such as mechanical testing, degradation analysis, *in-vitro* & *in-vivo* testing, and surface chemistry are needed for validation. Compressive mechanical testing is needed for validating the loading conditions covered in the simulation, as well as establishing if any issues are present in the implant that the design and simulation overlooks. Furthermore, a redesign of the implant can be done based on the data from mechanical testing. Degradation analysis with more extensive ICP-AES as well as profilometry will allow for a more accurate estimation of degradation rates, which in turn need to be compared with the growth rate of stem cells that are seeded on the implant. The rates must match up so that as the implant degrades, the growing stem cells differentiate into osteoblasts and fill in the vacancy. Profilometry will also give more information about the depth changes with time, as well as porosity data, which can be used to alter the design if needed to control degradation better.

On the biological side, additional in-vitro testing is needed to study the differentiation activity of the stem cells as they need to differentiate into osteoblasts. For this, five different tests need to be performed: MTT to evaluate the viability, confocal and SEM imaging to evaluate the cellular activity on the surfaces of the implant, and Alkaline phosphatase (ALP) test to evaluate the degree of differentiation seen in the cells, and Polymerase Chain Reaction (PCR) to evaluate the gene expression from the differentiation. Only with adequate data from these tests can the implant be considered ready for *in-vivo* application. For such an implant, the *in-vivo* application needs to be performed in gradual steps. The first step will focus purely on the viability of the implant within the body, with implantation on cranial defects in the rat. Once they are assessed based on histology and micro-CT of the implant after it has been successfully implanted for at least 6 weeks, the *in-vivo* study can move on to the next step: higher animals such as goats or sheep. The implant can now be also tested for functionality, with implantation on a goat or sheep femur. These animals are selected based on the high load and pressures their limbs need to sustain. Only after successful implantation in such animals, can the implant move towards clinical trials. Just fabrication is not enough, and these experimental techniques are key for ensuring that the implant is well designed and well tested, giving a robust 3D printed, biodegradable metal implant for bone regeneration.

Summary

Research on fracture healing for load-bearing bones has come a long way from the use of simple splints to keep a foot straight while it attempts to realign and heal adequately. Modern research is focused more on internally aiding the bone to heal correctly, via the use of medical devices such as rods, plates, and implants. While several examples exist that have attempted to make implants for such a functionality, the novelty in this paper lies in integrating features to be desirable in a scaffold, like load bearing, biodegradability, biocompatibility, and osseointegration focused on good clinical translation. This paper covers the use of appropriate materials based on several features that one can desire in such an implant and the use of dopants to enhance certain properties. Furthermore, it gives an overview of the design and fabrication of such an implant along with some experimental analysis. With such an approach toward creating a robust implant that balances fabrication and biocompatibility, it has the potential to improve iteratively, and in time succeed current methods for healing critical defects in load-bearing bones.

References

[1] R. Marti, "Fractures of the Lower Leg," in *Treatment of Fractures in Children and Adolescents*, Springer, Berlin, Heidelberg, 1980, pp. 330–349.

[2] S. Morshed and A. Ding, "Fracture healing," *Nonunions Diagnosis, Eval. Manag.*, pp. 45–74, Sep. 2017.

[3] J. J. Li *et al.*, "A Novel Bone Substitute with High Bioactivity, Strength, and Porosity for Repairing Large and Load-Bearing Bone Defects," *Adv. Healthc. Mater.*, vol. 8, no. 8, p. 1801298, Apr. 2019.

[4] E. Roddy, M. R. DeBaun, A. Daoud-Gray, Y. P. Yang, and M. J. Gardner, "Treatment of critical-sized bone defects: clinical and tissue engineering perspectives," *European Journal of Orthopaedic Surgery and Traumatology*, vol. 28, no. 3. Springer, pp. 351–362, 28-Oct-2018.

[5] J. L. Kelsey and E. J. Samelson, "Variation in risk factors for fractures at different sites," *Current Osteoporosis Reports*, vol. 7, no. 4. Springer, pp. 127–133, 29-Nov-2009.

[6] M. L. Wolford, K. Palso, A. Bercovitz, and P. D. Monica L. Wolford, M.A.; Kathleen Palso, M.A.; and Anita Bercovitz, M.P.H., "Hospitalization for Total Hip Replacement Among Inpatients Aged 45 and Over: the United States, 2000–2010," *Nchs*, no. 186, p. 8, 2015.

[7] N. Sudarmadji, J. Y. Tan, K. F. Leong, C. K. Chua, and Y. T. Loh, "Investigation of the mechanical properties and porosity relationships in selective laser-sintered polyhedral for functionally graded scaffolds," *Acta Biomater.*, vol. 7, no. 2, pp. 530–537, 2011.

[8] B. Hanks, S. Dinda, and S. Joshi, "Redesign of the femoral stem for a total hip arthroplasty for additive manufacturing," in *ASME International Design Engineering Technical Conferences and Computers and Information in Engineering Conference*, 2018, pp. 1–13.

[9] J. R. Denning, "Complications of Pediatric Foot and Ankle Fractures," *Orthopedic Clinics of North America*, vol. 48, no. 1. W.B. Saunders, pp. 59–70, 01-Jan-2017.

[10] U. Spiegl, R. Pätzold, J. Friederichs, S. Hungerer, M. Militz, and V. BüHren, "Clinical course, complication rate and outcome of segmental resection and distraction osteogenesis after chronic tibial osteitis," *Injury*, vol. 44, no. 8, pp. 1049–1056, Aug. 2013.

[11] R. M. Pilliar, J. E. Davies, and D. C. Smith, "The Bone-Biomaterial Interface for Load-Bearing Implants," *MRS Bull.*, vol. 16, no. 9, pp. 55–61, 1991.

[12] T. Wehner, L. Claes, and U. Simon, "Clinical Biomechanics Internal loads in the human tibia during gait," *Clin. Biomech.*, vol. 24, no. 3, pp. 299–302, 2009.

[13] A. R. Amini, C. T. Laurencin, and S. P. Nukavarapu, "Bone tissue engineering: Recent advances and challenges," *Crit. Rev. Biomed. Eng.*, vol. 40, no. 5, pp. 363–408, 2012.

[14] G. Fernandez de Grado *et al.*, "Bone substitutes: a review of their characteristics, clinical use, and perspectives for large bone defects management," *Journal of Tissue Engineering*, vol. 9. SAGE Publications Ltd, 02-Jun-2018.

[15] S. N. Khan, F. P. Cammisa, H. S. Sandhu, A. D. Diwan, F. P. Girardi, and J. M. Lane, "The biology of bone grafting.," *The Journal of the American Academy of Orthopaedic Surgeons*, vol. 13, no. 1. pp. 77–86, 2005.

[16] S. Bose, S. Vahabzadeh, and A. Bandyopadhyay, "Bone tissue engineering using 3D printing," *Mater. Today*, vol. 16, no. 12, pp. 496–504, 2013.

[17] D. Hong *et al.*, "Binder-jetting 3D printing and alloy development of new biodegradable Fe-Mn-Ca/Mg alloys," *Acta Biomater.*, vol. 45, pp. 375–386, 2016.

[18] P. Chocholata, V. Kulda, and V. Babuska, "Fabrication of scaffolds for bone tissue regeneration," *Materials*, vol. 12, no. 4. MDPI AG, 14-Feb-2019.

[19] R. Karunakaran, S. Ortgies, A. Tamayol, F. Bobaru, and M. P. Sealy, "Additive manufacturing of magnesium alloys," *Bioactive Materials*, vol. 5, no. 1. KeAi Communications Co., pp. 44–54, 01-Mar-2020.

[20] M. Prakasam, J. Locs, K. Salma-Ancane, D. Loca, A. Largeteau, and L. Berzina-Cimdina, "Biodegradable materials and metallic implants-A review," *Journal of Functional Biomaterials*, vol. 8, no. 4. MDPI AG, 26-Sep-2017.

[21] T. Kraus *et al.*, "Biodegradable Fe-based alloys for use in osteosynthesis: Outcome of an in vivo study after 52 weeks," *Acta Biomater.*, vol. 10, no. 7, pp. 3346–3353, 2014.

[22] R. Home, “Engineering Software Designed for Advanced Manufacturing | nTopology,” 2020. [Online]. Available: https://ntopology.com/. [Accessed: 17-Jun-2020].
[23] “Long Bone Structure - Human Anatomy Chart.” [Online]. Available: https://www.anatomylibrary99.com/. [Accessed: 17-Jun-2020].
[24] A. Wall and T. Board, “The compressive behavior of bone as a two-phase porous structure,” in *Classic Papers in Orthopaedics*, 2014, pp. 457–460.
[25] “ExOne | Metal 3D Printing Materials & Binders,” 2020. [Online]. Available: https://www.exone.com/en-US/3d-printing-materials-and-binders/metal-materials-binders. [Accessed: 09-Jun-2020].
[26] A. Mostafaei, P. Rodriguez De Vecchis, I. Nettleship, and M. Chmielus, “Effect of powder size distribution on densification and microstructural evolution of binder-jet 3D-printed alloy 625,” *Mater. Des.*, vol. 162, pp. 375–383, Jan. 2019.
[27] Y. F. Zheng, X. N. Gu, and F. Witte, “Biodegradable metals,” *Materials Science and Engineering R: Reports*, vol. 77. Elsevier Ltd, pp. 1–34, 01-Mar-2014.
[28] Y. F. Zheng, *Magnesium Alloys as Degradable Biomaterials-CRC Press (2015)*. 2016.
[29] M. Sabzi and M. Farzam, “Hadfield manganese austenitic steel: A review of manufacturing processes and properties,” *Mater. Res. Express*, vol. 6, no. 10, 2019.
[30] A. 52900:2015, “Standard Terminology for Additive Manufacturing – General Principles – Terminology,” *ASTM Int.*, vol. I, pp. 1–9, 2015.
[31] “Binder Jetting Powder Size Distribution.” [Online]. Available: https://additivenews.com/team-researchers-explains-effect-powder-size-distribution-binder-jetting-steel/.
[32] V. K. Ganesh, K. Ramakrishna, and D. N. Ghista, “Biomechanics of bone-fracture fixation by stiffness-graded plates in comparison with stainless-steel plates,” *Biomed. Eng. Online*, vol. 4, p. 46, Jul. 2005.
[33] M. Schinhammer, A. C. Hänzi, J. F. Löffler, and P. J. Uggowitzer, “Design strategy for biodegradable Fe-based alloys for medical applications,” *Acta Biomater.*, vol. 6, no. 5, pp. 1705–1713, 2010.
[34] L. Bai *et al.*, “Additive manufacturing of customized metallic orthopedic implants: Materials, structures, and surface modifications,” *Metals*, vol. 9, no. 9. MDPI AG, p. 1004, 01-Sep-2019.
[35] N. Eliaz, “Corrosion of metallic biomaterials: A review,” *Materials*, vol. 12, no. 3. MDPI AG, 28-Jan-2019.
[36] A. Kawecki *et al.*, “Fabrication, properties and microstructures of high strength and high conductivity copper-silver wires,” *Arch. Metall. Mater.*, vol. 57, no. 4, pp. 1261–1270, 2012.
[37] W. E. Frazier, “Metal additive manufacturing: A review,” *J. Mater. Eng. Perform.*, vol. 23, no. 6, pp. 1917–1928, 2014.
[38] S. Vangapally, K. Agarwal, A. Sheldon, and S. Cai, “Effect of Lattice Design and Process Parameters on Dimensional and Mechanical Properties of Binder Jet Additively Manufactured Stainless Steel 316 for Bone Scaffolds,” *Procedia Manuf.*, vol. 10, pp. 750–759, 2017.